Polymer 54 (2013) 1530–1537

Contents lists available at SciVerse ScienceDirect

Polymer

journal homepage: www.elsevier.com/locate/polymer

Plane stress local failure criterion for polycarbonate containing laser drilled microvoids

Trevor Meunier, Sai Gautam Gopalakrishnan, A. Weck*

Mechanical Engineering Department, University of Ottawa, Ottawa, Ontario, Canada K1N6N5

A R T I C L E I N F O

Article history:
Received 28 November 2012
Received in revised form
12 January 2013
Accepted 19 January 2013
Available online 28 January 2013

Keywords:
Fracture
Femtosecond laser microvoids
Finite element simulations

A B S T R A C T

The deformation and fracture mechanisms of voided polymers and rubber-toughened polymers are an active research area where accurate fracture models still need to be proposed. The reason for the lack of accurate models stems from a lack of controlled experiments at the microscale, the scale of voids and cracks forming in polymers. In this paper, controlled experiments were carried out on thin polycarbonate sheets containing controlled arrays of laser microvoids, loaded in-situ under an optical microscope. Void dimensions were extracted experimentally and compared to a simple finite element model that was able to accurately predict macroscopic stress strain curves as well as the microscopic behavior in terms of void growth. It is shown that the local equivalent plastic strain at failure is independent of the void configuration studied and can therefore be used as a criterion for predicting fracture in voided polycarbonate under plane stress. We propose that it is not the intervoid spacing that controls fracture but the competition between intervoid strain localization and the spread of plasticity through the propagation of shear bands.

1. Introduction

Polymers have engineering applications in various industries including electronic, automotive and medicine. However their usage has been largely constrained by their tendency to fracture in a brittle manner especially at low temperatures and high strain rates. In order to increase the fracture toughness of polymers, a rubber-like phase can be introduced. Previous experimental studies [1,2] have indicated the importance of void initiation, or "cavitation", and growth at such rubber-like phases in the toughening of polymers. Cavitation leads to a reduction in the hydrostatic component of the stress tensor and bulk modulus around the void thus leading to an increase in the deviatoric component of the stress tensor and an increased plastic flow, a phenomenon referred to as 'shear yielding'. Also, a very high resistance to cavitation might lead to crazing and in turn brittle fracture. Hence, it is imperative to build knowledge about the process of void nucleation and growth in order to critically understand fracture processes in a polymer.

Deformation of polymer-rubber blends can be split into two distinct processes, (i) cavitation occurring in the rubber particles and (ii) yielding in the cavitated polymer. It was suggested that plastic void growth is the most dominant toughening mechanism in rubber-toughened polymers irrespective of the particle size (even in the "nano" regime), particularly for high bulk modulus and high rigidity particles [3]. It was also demonstrated that tests on samples containing rubber modifiers with different cavitation resistance or containing hollow plastic micro-spheres which act as pre-existing microvoids toughen epoxies in the same manner [4]. Recent studies [5–7] have therefore replaced the rubber particles by equivalent spherical voids in their numerical models. This is because post-cavitation, the soft rubber particles do not contribute significantly to the plastic deformation of the matrix and hence can be replaced by spherical voids of void fraction equal to the initial rubber volume fraction. The polymer-rubber blend thus imitates the deformation behavior of a porous polymer where plastic deformation is encouraged in the ligaments between the voids. To predict polymer fracture, it is therefore necessary to understand void growth and thus plasticity in polymers. Unlike plasticity in metals, polymers show significant softening right after yield followed by drastic hardening at large strains. The softening behavior is attributed to the evolution of large free volume associated with certain metastable states and the hardening behavior is explained by the orientation of polymeric chains and the stretching of the entangled polymer network. Therefore polymers are highly prone to strain localization, propagation of shear bands and necking. There have been models to imitate this stress-strain behavior of polymers including piece-wise linear functions [8], visco-plastic constitutive equations with a back stress based on three-

* Corresponding author.
E-mail address: aweck@uottawa.ca (A. Weck).

0032-3861/$ – see front matter © 2013 Published by Elsevier Ltd.
http://dx.doi.org/10.1016/j.polymer.2013.01.031

dimensional orientation distribution of molecular chains in a non-Gaussian network [7] and a flow stress model [9].

In terms of defining fracture criteria for polymers, various macroscopic criteria based on parameters like the J-integral [10], the equivalent elongation concept for rubber-like polymers under plane stress conditions [11], strain energy [12,13] and an invariant strain criterion [14] have been defined. Since the process of cavitation, void growth and toughening along the ligaments linking the voids are all microscopic processes dependent on local stress and strain conditions rather than the far field ones, it is imperative to estimate fracture using criteria derived locally. Previous attempts to study the local deformation behavior of polymers have been done with methods such as x-ray tomography [15], x-ray scattering [16,17], digital image correlation [18,19], Moiré interferometry [20], finite element simulations [15,20] and molecular modeling [21]. However, except for a few like [17], there have not been many in-situ studies of fracture processes in polymers.

In this paper, we conducted in-situ experiments and finite element simulations on polycarbonate to study void growth and coalescence in order to extract a local fracture criterion. Polycarbonate foils containing micron-sized voids machined using a femtosecond pulsed laser were subject to in-situ tensile deformation under an optical microscope. Finite element simulations were then performed in order to extract the local stress and strain values corresponding to the failure of the material.

2. Experimental methods

Tensile coupons were machined out of a 175 μm thick, extruded, isotropic, polycarbonate film purchased from Goodfellow (*Bayer Makrofol Grade DE 1-1*). The tensile coupons had a dog-bone shape with a gage length of 5 mm and a gage width of 1 mm. Each tensile coupon had a series of cylindrical through voids machined across the width of the gage length. The voids were machined with a femtosecond pulsed laser in order to produce voids with a negligible heat affected zone. This laser machining approach has recently been developed to study fracture in metals [22–25]. The voids diameter was measured to be on average 20 μm. Six different void configurations were tested and are summarized in Table 1. The void configurations consisted of either one line with voids along the width of the sample or two lines where the voids made an angle of 45° with respect to the tensile direction. In both cases, three void spacings were considered, 50 μm, 75 μm, and 100 μm in order to obtain volume fractions of voids similar to that found in rubber-toughened polymers, i.e. 20%–40% [27]. Samples were loaded in tension with a micro-tensile tester (*MTI Instruments SEM tester18246-SEM*) at a speed of 4.8 μm/s resulting in a strain rate of approximately 1×10^{-3} s^{-1}. It should be noted that the local strain rate between the voids will be higher than the global strain rate. When the shear band forms between the voids we can assume that all the deformation is localized in the voids region. The local strain rate is then the test speed (4.8 μm/s) divided by the voids diameter (20 μm) which gives a strain rate of 0.24 s^{-1}. Based on experimental data on polycarbonate obtained by Fleck et al. [26], a change in strain rate from 1×10^{-3} s^{-1} to 0.24 s^{-1} would result in only small changes in yield strength and failure strains. Strain rate effects have therefore not been included in our study. The micro-tensile tester also allowed for both load and displacement to be recorded during the test in order to obtain a stress strain curve for each void configuration. Tensile tests were carried out in-situ under an optical microscope (*Nikon Optiphot-100*) and images were acquired during the tensile test at a rate of 3 images per second. Images acquired for each tensile test were used to extract the dimensions of each void throughout the course of the test using the ImageJ program, a Java-based open-source software (http://imagej.nih.gov/ij/). Dimensions of a bounding rectangle around each void were exported allowing for the results to be easily analyzed and compared. The main values of interest were the initial void diameter a_0 in the tensile direction and the initial void diameter in the transverse direction b_0 as well as the instantaneous void diameters a and b in the tensile and transverse directions respectively.

Table 1
Void configurations machined in the gage of polycarbonate samples.

Sample name	Condition	Smallest void spacing [μm]	Void spacing normal to tensile direction [μm]	Number of voids in sample	Void volume fraction [%]
50mic	1 line	50	50	19	40.0
50mic45	2 lines	50	71	27	28.2
75mic	1 line	75	75	13	26.7
75mic45	2 lines	75	106	17	18.9
100mic	1 line	100	100	10	20.0
100mic45	2 lines	100	141	13	14.2

3. Experimental results

Engineering stress-strain curves were obtained for each sample and are presented in Fig. 1. They show typical polymeric behavior with a linear elastic region, a yield point, and a strain softening region followed by rehardening as straining progresses. The larger the spacing between the voids, the larger the engineering failure strain is. The 75 μm and 100 μm cases have similar failure strains while the 50 μm cases have much lower failure strains. There are also no significant differences between the 1 line case and the 2 lines case with voids at 45°. A typical deformation sequence is shown in Fig. 2 where images were taken from the center of the gage length for a sample with 2 lines of voids at 45° and smallest void spacing of 75 microns. The voids are initially circular (Fig. 2(a)) and elongate as the deformation band starts forming between the voids (Fig. 2(b)). Propagation of the band through the voids results in extensive void growth (Fig. 2(c and d)). Very little growth is observed during band propagation through the gage length as most of the deformation takes place away from the voids (Fig. 2(e)). Once the band has finished propagating through the entire gage length, cracks start forming at the equator of the voids leading to the final failure of the sample (Fig. 2(f)).

Fig. 3 shows the last image recorded before final failure of the material. All configurations fail by the formation of a crack at the equator of the voids. It is interesting to note that even though the voids are spaced closer to each other for the cases with voids at 45°, fracture takes place normal to the tensile direction. This effect is particularly striking for the 50 μm case (Fig. 3(b)) where the ligament between the voids has thinned down significantly at 45° compared to the ligament normal to the tensile axis and yet the sample fails normal to the tensile axis.

Major and minor void dimensions were extracted for all void configurations and are presented in Fig. 4. The growth of the major diameter (a/a_0) initially accelerates over a small amount of plastic strain (<0.1) leading to a very steep void growth corresponding to the nucleation and propagation of the deformation band through the voids region. During this process the major diameter of the voids experiences a 3–3.5 times increase. For the 50 μm case with 1 line of voids, failure takes place before the deformation band has time to propagate fully through the line of voids. For the 50 μm case with voids at 45°, the deformation band propagates through the voids but the sample fails shortly afterwards. For all other void configurations (75 μm and 100 μm), the initial band propagation through the voids is followed by a relatively slow void growth over a large amount of strain, up to an engineering

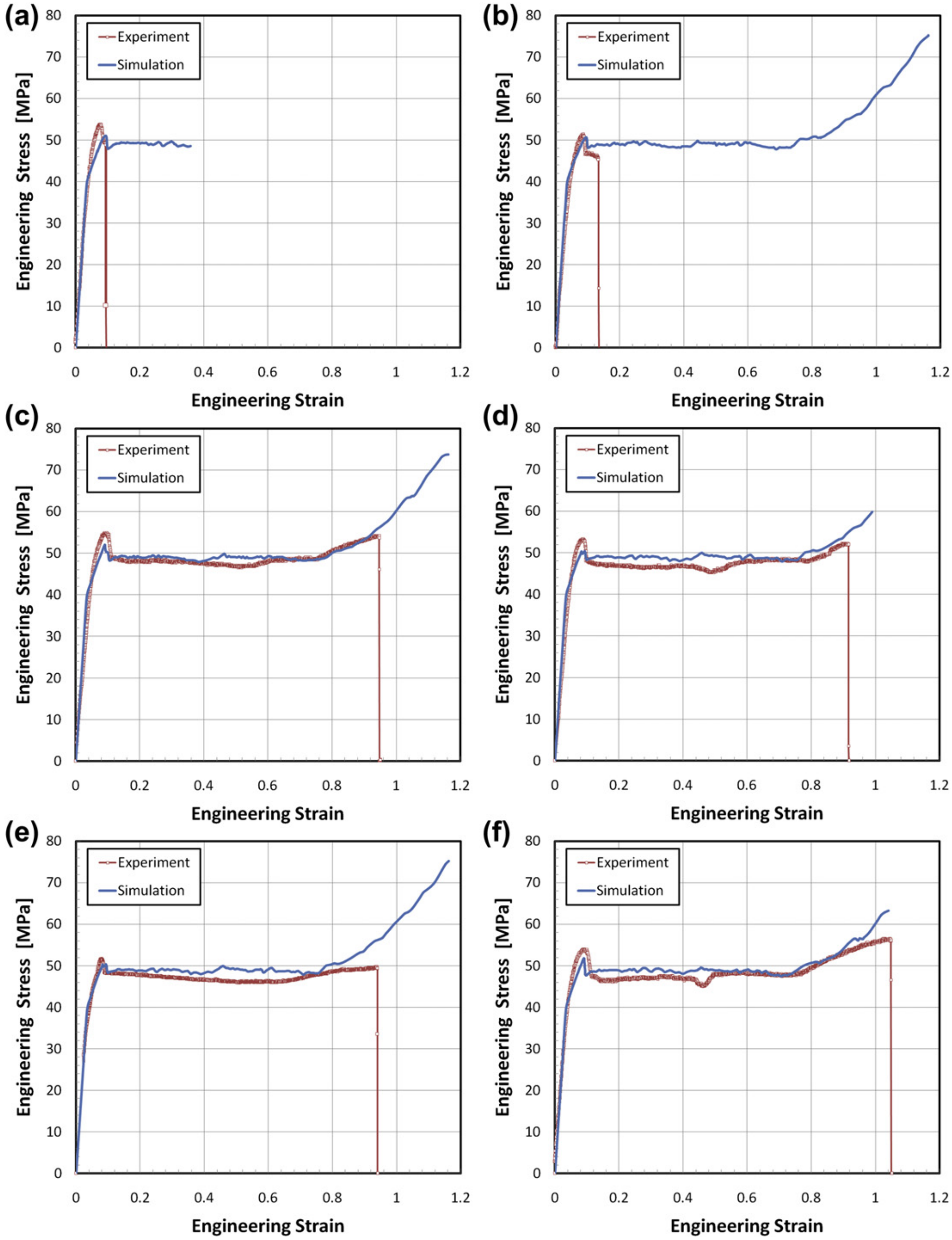

Fig. 1. Experimental and finite element engineering stress strain curves for various void configurations: a) 50mic, b) 50mic45, c) 75mic, d) 75mic45, e) 100mic and f) 100mic45. (Refer to Table 1 to relate sample name to void configuration).

strain value of approximately 1. This slow growth takes place while the deformation band propagates through the entire gage length of the sample. Void growth finally accelerates again close to fracture after the deformation band has propagated through the sample and when deformation localizes again in the voids region.

The evolution of the minor void diameter (Fig. 4) shows an initially constant value followed by a peak during band propagation where the diameter initially increases and then decreases again. The peak is more pronounced for lines of voids as opposed to voids at 45° (Fig. 4) and the closer the voids are to each other which is probably due to the stronger interactions between voids. After the peak, all curves show a slight decrease in minor diameter until close to fracture where void growth increases significantly as a result of the formation of cracks at the equator of the voids.

4. Finite element simulations

Simulations were carried out with Abaqus/Standard [30] within the framework of the finite deformation theory with the initial unstressed state as reference. Linear 8-node brick elements with reduced integration (C3D8R) were used for a total going from 55,000 to 75,000 elements depending on the void geometry. The

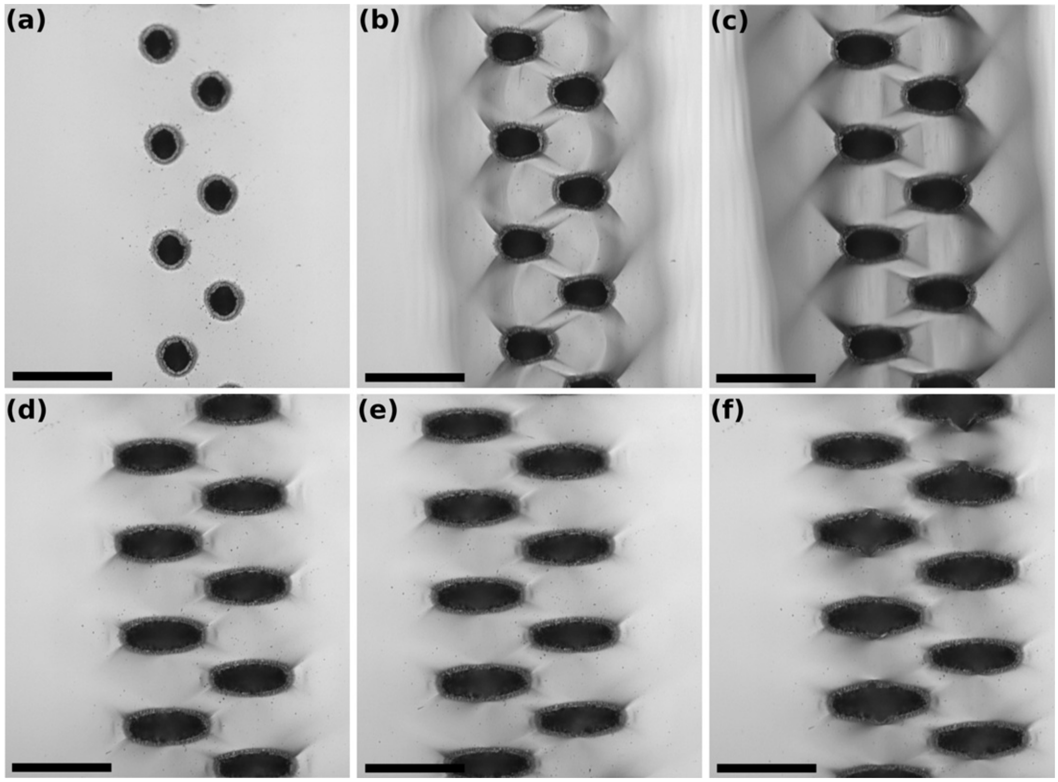

Fig. 2. Optical microscope images of the void growth sequence for sample 75mic at engineering strains of a) 0, b) 0.093, c) 0.097, d) 0.148, e) 0.570, f) 0.894. Tensile axis is horizontal. Scale bar is 100 μm (Refer to Table 1 to relate sample name to void configuration).

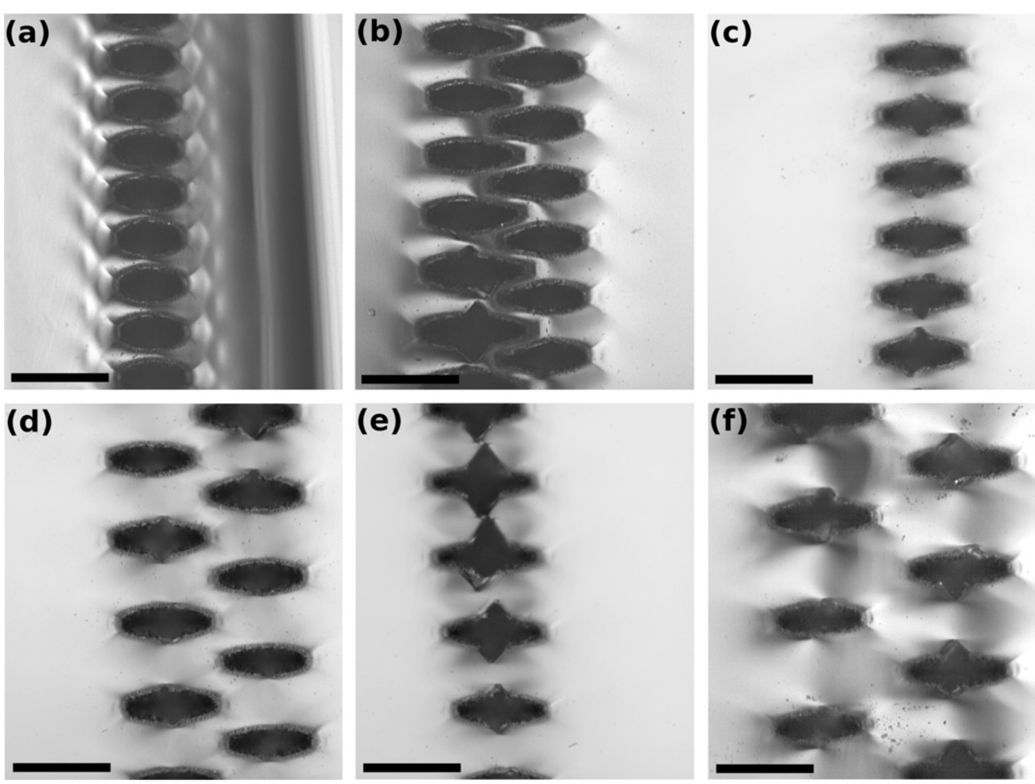

Fig. 3. Optical microscope images taken at incipient fracture between the void for various void configurations: a) 50mic, b) 50mic45, c) 75mic, d) 75mic45, e) 100mic and f) 100mic45. Tensile axis is horizontal. Scale bar is 100 μm (Refer to Table 1 to relate sample name to void configuration).

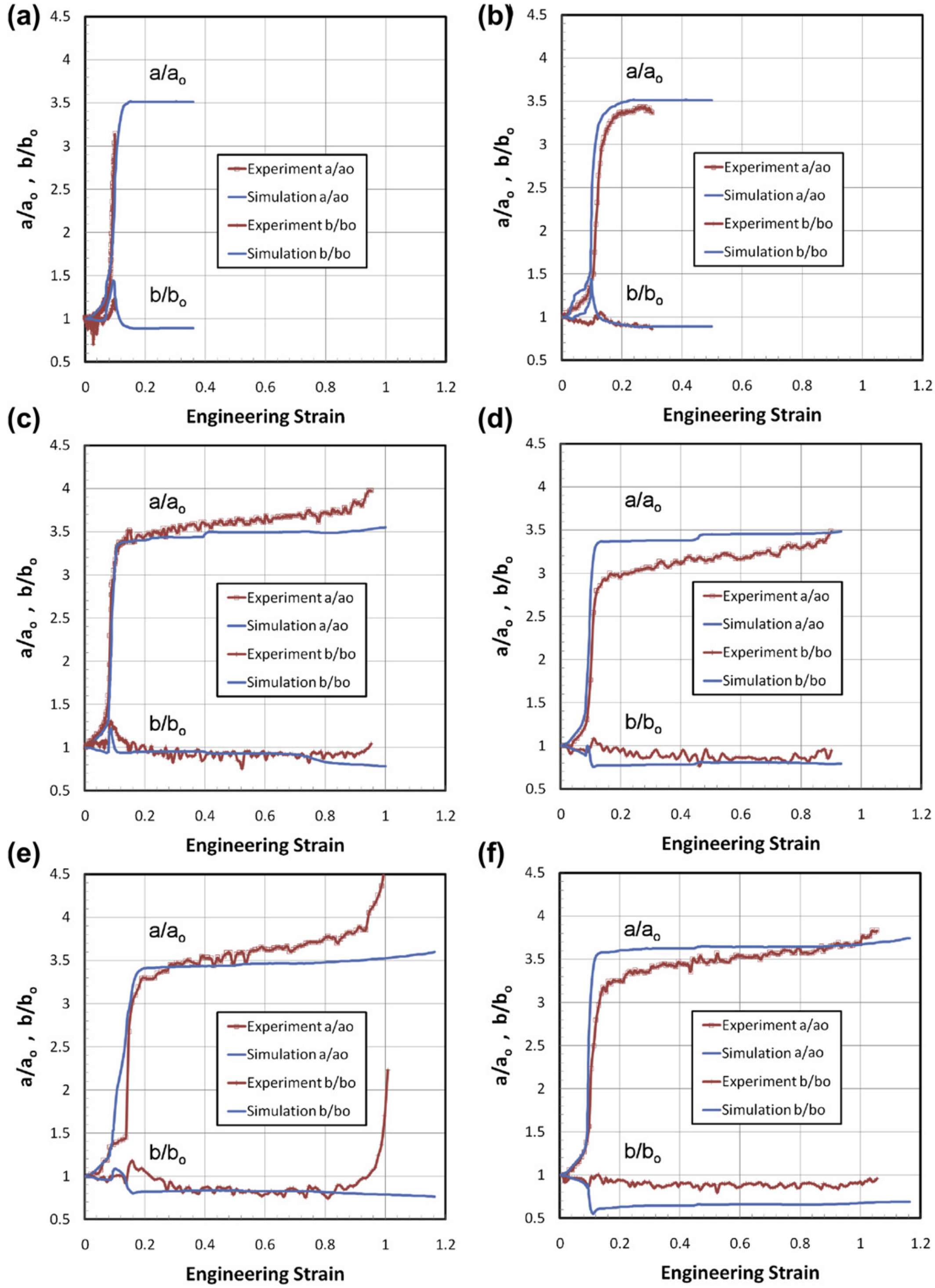

Fig. 4. Major (a/a_0) and minor (b/b_0) void diameters obtained experimentally and from the finite element simulations for various void configurations: a) 50mic, b) 50mic45, c) 75mic, d) 75mic45, e) 100mic and f) 100mic45. (Refer to Table 1 to relate sample name to void configuration).

three-dimensional finite element model reproduced the entire tensile sample and the mesh was refined close to the voids as shown in Fig. 5. A mesh sensitivity analysis was performed to ensure no mesh size dependence of the results.

Polycarbonate was modeled as a rate and temperature independent isotropic, elasto-plastic solid following the J_2 theory of plasticity with isotropic hardening. The elastic constants were $E = 2350$ MPa and $\nu = 0.37$, and the flow stress, σ, was treated as a function of the accumulated plastic strain, ε_p, using values shown Table 2, similar to those found in Ref. [8]. The sample was deformed by applying an equal and opposite displacement at each end of the sample along the x-direction in Fig. 5. Stress strain curves were obtained for each void configuration tested experimentally and are shown in Fig. 1 along with the experimental results. The predictions are in very good agreement with the experiments where yield point, softening, band propagation and rehardening are well predicted,

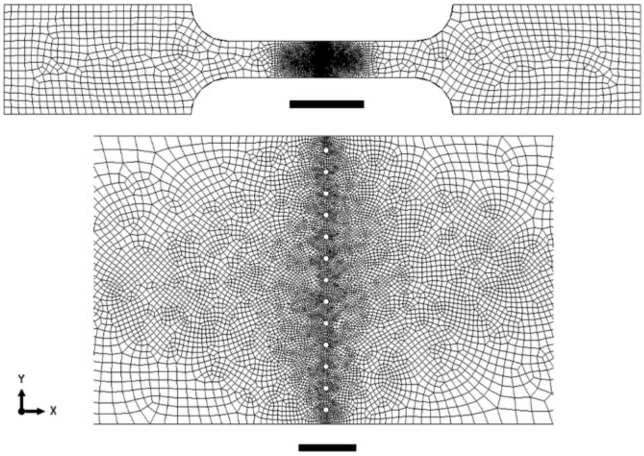

Fig. 5. Finite element mesh (top) with a magnified view of the middle of the gage length (bottom) showing a configuration of voids identical to the experimental one. Top scale bar is 2 mm and bottom one is 200 μm.

validating the constitutive law chosen for polycarbonate. Void growth behavior (Fig. 6) qualitatively agrees with that observed experimentally (Fig. 2) and major and minor void diameters were extracted and compared to experimental results in Fig. 4. The evolution of both major and minor diameters is well predicted in terms of strain as well as extent of void growth. As there is no failure criterion in the simulation, the final failure strains were not predicted. In order to better understand what controls failure in this material, finite element simulations were ran until a far field engineering strain corresponding to the experimental failure strain. It is assumed here that the coalescence (or crack initiation) strain is equal to the failure strain because once the crack starts forming, failure proceeds over a negligible amount of far field engineering strain. Once the simulation reached the experimental failure strain, various local parameters were extracted from the simulation, including the maximum plastic equivalent strain and the maximum Von Mises equivalent stress. Among these parameters, is was found that the maximum plastic equivalent strain at failure was essentially independent of the void configuration with an average value of 1.35 and a standard deviation of 0.03 as shown in Fig. 7.

5. Discussion and conclusion

The results presented in this paper show the first controlled microscale in-situ study of void growth and coalescence in a polymer. The advantage of using a femtosecond laser to machine the voids is that it produces a negligible heat affected zone compared to the size of the voids which allows to mimic voids forming in real materials. Furthermore the sample being placed on a translation stage during laser machining allows precise control over the position of the voids. This allowed us to accurately compare experimental results to finite element simulations and deduce local failure strains for various void configurations including different spacings (or void volume fractions) and void orientations with respect to the tensile axis. The constitutive law used in the finite element model is very simple and is able to capture the main effects observed experimentally for various void configurations such as strain softening and rehardening, deformation band formation and void growth evolution.

Table 2
Plastic properties of polycarbonate used in the finite element simulations.

Stress [MPa]	Plastic strain
40	0
55	0.05
45	0.25
50	0.8
110	1
800	3

Interestingly, the various void volume fractions studied in this paper were seen to affect the macroscopic failure strains but do not appear to affect the macroscopic stress levels on the stress strain curves. This is due to the fact that once the stress reaches the yield point, it cannot increase until the rehardening stage. Whether the voids are close or far from each other, the stress that needs to be reached locally to have yielding is the same. On the contrary, the deformation required to have yielding between the voids will depend on the void spacing where it is expected to have more deformation before yielding when the voids are further away from each other. However, in our experiments, there is only one or two lines of voids which means that the contribution of the local deformation between the voids to the overall deformation is negligible, hence the lack of difference between the different stress levels. The finite element simulation confirmed that the stress level is indeed not affected by the void volume fraction in this study.

Another interesting feature is the peak in minor diameter observed both experimentally and in the finite element simulations (Fig. 4). To better understand this phenomenon, the stress triaxiality in an element in the middle of the ligament between the voids is presented in Fig. 8. The stress triaxiality is defined as the mean stress σ_m (where $\sigma_Y = (\sigma_1 + \sigma_2 + \sigma_3)/3$) over the equivalent Von-Mises stress σ_Y where ($\sigma_Y^2 = 1/2[(\sigma_1 - \sigma_2)^2 + (\sigma_2 - \sigma_3)^2 + (\sigma_3 - \sigma_1)^2]$). The stress triaxiality increases rapidly during shear band propagation which is accompanied by a rapid increase in the minor void diameter. As the stress triaxiality starts to decrease, the rate of minor void growth slowly decreases, the void diameter reaches a maximum and the void growth rate becomes negative with further decrease in stress triaxiality. It is therefore the high stress triaxiality imposed by the shear band that is responsible for the peak in minor void diameter.

The laser machining approach allows a precise control over the void volume fraction, which was varied by changing the intervoid spacing. It was found that for configurations with void spacings equal to or larger than 75 μm, the initial strain localization between voids is followed by shear band propagation over the entire sample gage length. On the contrary, for void spacings of 50 μm, strain localization between voids resulted in the final failure of the sample before the shear band had a chance to propagate along the gage length. Because the finite element model was able to reproduce both macro- and microscopic behaviors quantitatively, it was also possible to extract the local failure strains in the ligaments between voids. We found that independently of the void configuration, the samples always failed at an average local equivalent plastic strain of 1.35. It should be noted that the critical strain was only validated for the given set of experimental parameters used in this study, i.e. plane stress uniaxial tensile tests performed at room temperature at a strain rate of $1 \times 10^{-3}\ s^{-1}$ and that changing these parameters may change the critical strain. The approach presented here is however providing information on the competition between strain localization between voids and spread of the plasticity through shear band propagation. Such information is of critical importance for studies on rubber-toughened polymers where the void volume fraction can affect the type of failure observed. More specifically, it was found that the intervoid spacing is an important parameter controlling the toughness of rubber-toughened polymers where the polymer goes through a ductile to brittle transition with increasing intervoid spacing [4]. The same study has also shown that the critical intervoid spacing varies with reinforcement size,

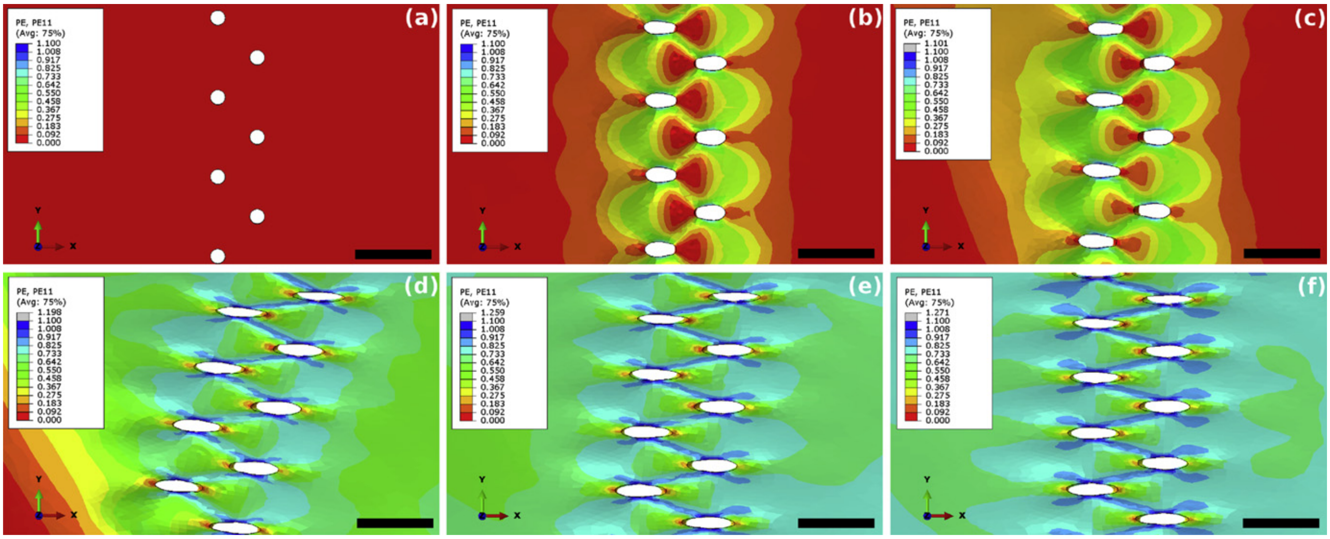

Fig. 6. Finite element simulation results showing void growth and the axial strain distribution in the tensile axis (horizontal) for sample 75mic45 at engineering strains of a) 0, b) 0.093, c) 0.097, d) 0.148, e) 0.570, f) 0.894. Scale bar is 100 μm.

a phenomenon that could be validated using the approach presented in this paper. We believe that it is not the intervoid spacing that controls fracture but rather whether a critical fracture strain is reached between the voids before plasticity is allowed to spread over the rest of the sample. If the local fracture strain between voids is reached while the shear band is still developing in the voided region, then fracture proceeds between the voids and a brittle fracture is obtained at the macroscale. If the shear can spread over the rest of the sample before the local failure condition is reached between the voids, then the sample can withstand much larger deformations and will have a ductile behavior. Changing parameters such as void size, intervoid spacing, void orientation, sample geometry, etc. will indirectly affect fracture because they affect the local strain required for failure. It is therefore important to obtain such local failure criteria to properly understand and model failure in polymeric materials.

This work demonstrated that important information can be gathered using laser micromachined model materials coupled with finite element simulations. More work is planned to look at the effects of stress state, temperature, and void size on void growth and fracture. It has been shown that the heterogeneity in void distribution can lead to sequential yielding which in turn results in a reduction or disappearance of the overall strain softening [29]. This effect can easily be studied using the approach presented in this paper by changing the randomness of the array of voids and observing its effect on strain softening and band propagation. Bimodal population of voids could also be investigated in a controlled manner as it was shown that biomodal void distribution increases the fracture toughness if the large voids can enlarge the crack tip plastic zone via branching mechanisms [28]. Finally, the voids presented in this study are cylinders going through the entire thickness of the sample. While finite element simulations can reproduce this void geometry, it does not represent real voids forming in materials during fracture which are generally spherical. It would therefore also be beneficial to carry out similar experiments where the voids would be spheres in the bulk of the material. By focusing the laser beam inside the polymer, it was recently demonstrated that microvoids can be obtained in the bulk [31], enabling more realistic studies on void growth and fracture mechanisms in polymers.

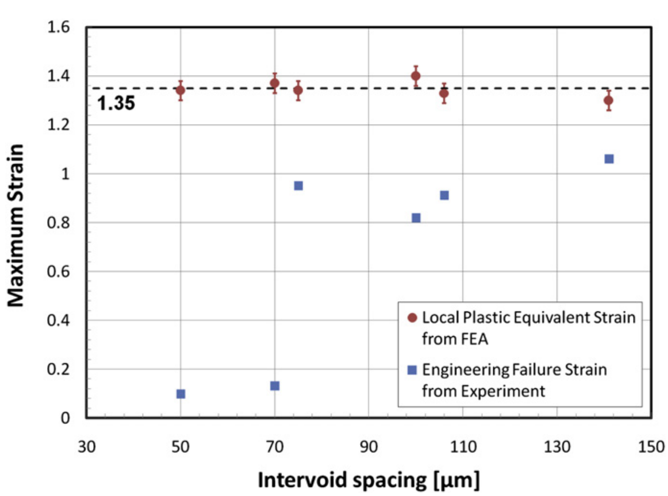

Fig. 7. Critical strain at fracture obtained experimentally and the corresponding maximum local plastic equivalent strain between the voids obtained from the finite element simulations as a function of initial void spacing.

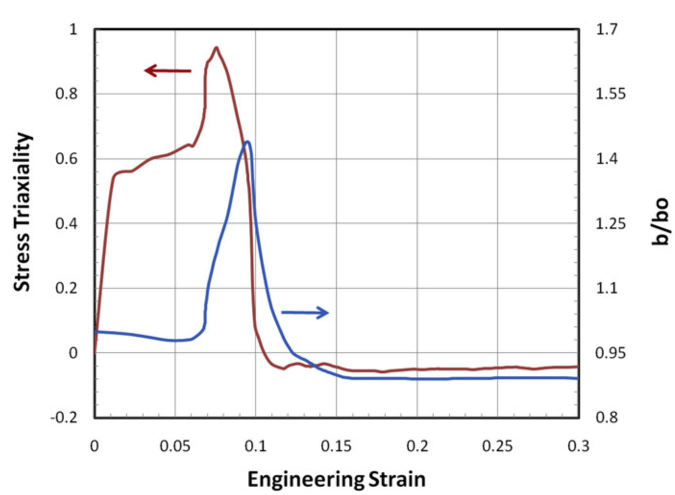

Fig. 8. Evolution of the stress triaxiality in the ligament between voids and the minor void diameter versus applied engineering strain for sample 50mic. (Refer to Table 1 to relate sample name to void configuration).

Acknowledgments

We gratefully acknowledge the support of the Natural Sciences and Engineering Research Council of Canada (NSERC) and Prof. R. Bhardwaj for access to the femtosecond laser.

References

[1] Bucknall CB. Applied Science Publications, London; 1977.
[2] Donald AM, Kramer EJ. Journal of Applied Polymer Science 1982;27:3729–41.
[3] Williams JG. Composites Science and Technology 2010;70:885–91.
[4] Bagheri R, Pearson RA. Polymer 2000;41:269–76.
[5] Steenbrink AC, Van Der Giessen E. Journal of the Mechanics and Physics of Solids 1999;47:843–76.
[6] Belayachi N, Benseddiq N, Nait-Abdelaziz M, Hamdi A. Science and Technology of Advanced Materials 2008;9:025008.
[7] Steenbrink AC, Van Der Giessen E, Wu PD. Journal of the Mechanics and Physics of Solids 1997;45:405–37.
[8] Sue H-J, Yee AF. Polymer 1988;29:1619–24.
[9] Cheng L, Guo TF. International Journal of Solids and Structures 2007;44:1787–808.
[10] Nait-Abdelaziz M, Zairi F, Qu Z, Hamdi A, Ait Hocine N. Mechanics of Materials 2012;53:80–90.
[11] Hamdi A, Nait Abdelaziz M, Ait Hocine N, Heuillet P, Benseddiq N. Polymer Testing 2006;25:994–1005.
[12] Volokh KY. Mechanics Research Communications 2010;37:684–9.
[13] Guedes RM. Journal of Reinforced Plastics and Composites 2010;29:3041–7.
[14] Gosse JH, and Christensen S. Collection of technical papers – AIAA/ASME/ASCE/AHS/ASC structures structural dynamics and materials conference; 2001; p. 45–55.
[15] Sket F, Seltzer R, Molina-Aldareguia JM, Gonzalez C, Llorca J. Composites Science and Technology 2012;72:350–9.
[16] Schneider K, Zafeiropoulos NE, Stamm M. Advanced Engineering Materials 2009;11:502–6.
[17] Davies RJ, Zafeiropoulos NE, Schneider K, Roth SV, Burghammer M, Riekel C, et al. Colloid and Polymer Science 2004;282:854–66.
[18] Zhou Z, Chen P, Duan Z, Huang F. Strain 2012;48:326–32.
[19] Sadowski T, Marsavina L, Craciun EM, Knec M. Computational Materials Science 2012;52:231–5.
[20] Lilleheden L. International Journal of Adhesion and Adhesives 1994;14:31–7.
[21] Rottler J. Journal of Physics Condensed Matter 2009;21:463101.
[22] Weck A, Crawford THR, Borowiec A, Wilkinson DS, Preston SJ. Applied Physics A-Materials Science & Processing 2007;86:55–61.
[23] Weck A, Wilkinson DS, Maire E, Toda H. Advanced Engineering Materials 2006;8:469–72.
[24] Weck A, Wilkinson DS. Acta Materialia 2008;56:1774–84.
[25] Weck A, Wilkinson DS, Maire E, Toda H. Acta Materialia 2008;56:2919–28.
[26] Fleck NA, Stronge WJ, Liu JH. Proceedings of The Royal Society of London Series A-Mathematical and Physical Sciences 1990;429:459–79.
[27] Steenbrink AC, Van Der Giessen E, Wu PD. Journal of Materials Science 1998;33:3163–75.
[28] Bagheri R, Williams MA, Pearson RA. Polymer Engineering and Science 1997;37:245–51.
[29] Smit RJM, Brekelmans WAM, Meijer HEH. Journal of the Mechanics and Physics of Solids 1999;47:201–21.
[30] Abaqus 6.11. Users manual. ABAQUS Inc; 2011.
[31] Meunier T, Villafranca AB, Bhardwaj R, Weck A. Optics Letters 2012;37:3168–70.